ENGINEERING Information Technology & Electronic Engineering
https://www.academax.com/EITEE; https://www.engineering.org.cn
https://ieeexplore.ieee.org/xpl/RecentIssue.jsp?punumber=11344065
E-mail: eng.itee@zju.edu.cn

Engineering Journals
Available on IEEE Xplore®

Research Article

https://doi.org/10.1631/ENG.ITEE.2026.0110

Novel four-dimensional direct sequence spread spectrum waveform design based on prolate spheroidal wave functions

Zhichao XU[1,2,3], Faping LU[2,3]✉, Zhilin ZHANG[3,4], Zhongyang MAO[2,3], Dongkai YANG[1], Jiafang KANG[2,3], Fucheng YANG[2], Feng WANG[1]

[1]*Beihang University, Beijing 100191, China*
[2]*Naval Aeronautic University, Yantai 264001, China*
[3]*Shandong Key Laboratory of Sea-Air Information Perception and Processing Technology, Yantai 264001, China*
[4]*PLA 91206 Unit, Qingdao 266100, China*

Abstract: With its excellent anti-interference capability, low probability of interception, and code-division multiple access capability, direct sequence spread spectrum plays a crucial role in unmanned aerial vehicle swarm communications, high-precision ranging, and massive connectivity in beyond fifth-generation and sixth-generation networks. However, low spectral efficiency and poor energy concentration of conventional rectangular chip waveforms used in spread spectrum modulation make it difficult to meet the high-rate and high-sensitivity reception requirements of future systems. To address this issue, this study proposes a spread spectrum chip waveform design method based on prolate spheroidal wave functions (PSWFs). By constructing a set of four orthogonal PSWF-based chip waveforms, the proposed method enhances signal dimensionality and spectral efficiency under finite time–bandwidth product constraints. Furthermore, an equivalent low-pass filter structure is integrated to reduce implementation complexity. Theoretical analysis and simulation results demonstrate that the proposed waveform achieves approximately double the spectral efficiency of conventional waveforms while maintaining comparable error performance. It also exhibits superior anti-interference and anti-interception capabilities, providing a viable waveform design approach for next-generation spread spectrum communication systems.

Key words: Direct sequence spread spectrum; Prolate spheroidal wave functions; Chip waveform; Spectral efficiency; Anti-interference

1 Introduction

Direct sequence spread spectrum (DSSS) spreads the signal spectrum using pseudorandom sequences (Hui et al., 2026), thereby obtaining processing gains. DSSS offers excellent anti-interference capability, low probability of interception, and code-division multiple access (CDMA) performance, and has been widely deployed in military communications, satellite telemetry and control (Liu JC et al., 2025; Yan et al., 2026), and civil mobile communications (Su et al., 2021; Todorović et al., 2024; Liu MZ et al., 2025). With the emergence of new application scenarios, such as low-altitude unmanned aerial vehicle swarm communications (Jin Y et al., 2026), high-precision anti-interception ranging (Wang et al., 2026), and massive machine-type communications for beyond fifth-generation (B5G) and sixth-generation (6G) networks (Duan et al., 2025; Yang ZJ et al., 2026), systems must ensure reliable transmission in complex electromagnetic environments and pursue high spectral efficiency (Lu ZW et al., 2024) and energy concentration to support high-rate data transmission and high-sensitivity reception (Shao et al., 2026). However, conventional DSSS systems typically use rectangular pulses as chip waveforms; these pulses exhibit abrupt time-domain truncation and severe spectral spreading, which results in low spectral efficiency and elevated correlation sidelobes, impairing multipath resolution and detection performance (Oh and Moon, 2024).

In recent years, extensive research has focused on spread spectrum waveform optimization to enhance the energy concentration of spread spectrum modulation signals and system spectral efficiency. First, methods such as spread spectrum code optimization, chip waveform replacement, and waveform shaping have been adopted to improve the energy concentration and out-of-band suppression capability of DSSS signals. Examples include spread spectrum code

✉ Faping LU, lufaping@163.com
Zhichao XU, https://orcid.org/0009-0007-2524-457X
Faping LU, https://orcid.org/0000-0002-8172-0311
Zhilin ZHANG, https://orcid.org/0009-0006-1442-3735
Zhongyang MAO, https://orcid.org/0000-0001-6279-1627
Dongkai YANG, https://orcid.org/0000-0003-4642-4557
Jiafang KANG, https://orcid.org/0000-0003-4177-5622
Fucheng YANG, https://orcid.org/0000-0001-6088-6884
Feng WANG, https://orcid.org/0000-0002-9046-3388
CLC number: TN911.23

Received: Apr. 20, 2026; Revision accepted: Aug. 14, 2026;
Crosschecked: Sept. 4, 2026; Published online: Sept. 29, 2026

© The Authors 2026. Published by Zhejiang University Press Co., Ltd.
This is an open access article distributed under the terms of the CC BY-NC-ND license (https://creativecommons.org/licenses/by-nc-nd/4.0/)

designs (such as constant amplitude zero auto-correlation codes, low-sidelobe optimization codes, and multidimensional joint spread spectrum codes (Vangelista et al., 2024)), high-energy concentration chip waveforms (such as raised-cosine functions and half-sine wave functions (Dai et al., 2025)), and waveform shaping techniques (such as fractional Fourier transform-assisted waveforms and constant-envelope waveforms (Yang YX and Gao, 2023)). Second, methods such as composite waveform construction, higher-order modulation, and multidomain joint optimization enhance the spectral efficiency and information transmission efficiency of DSSS systems. Examples include composite waveforms such as DSSS-based orthogonal frequency division multiplexing (Waheed and Mohammady, 2024), higher-order modulation fusion such as DSSS-based quadrature phase shift keying (Jin Y and Ji, 2011), and multidomain joint optimization such as reconfigurable intelligent surface-assisted time–frequency code codesign (Jin XP et al., 2023). Therefore, the key to improving spread spectrum system performance involves enhancing the signal energy concentration within limited time–frequency resources and expanding the information mapping dimensionality. Compared with common enabling technologies, such as spread spectrum code optimization, waveform shaping, higher-order modulation, and multidomain joint optimization, chip waveform replacement enhances energy concentration (Du et al., 2025; Huang et al., 2025; Han et al., 2026; Ni et al., 2026) and expands information mapping dimensionality (De Sanctis et al., 2015; Xue and Xie, 2023; Xu YZ et al., 2026). Furthermore, this approach can be combined with the above enabling technologies (Cai et al., 2025; He et al., 2025; Qian et al., 2025; Sarwar et al., 2025; Dogukan and Basar, 2026) to achieve additional system performance gains. Moreover, among various signals with high-energy concentration, prolate spheroidal wave functions (PSWFs) have attracted increasing attention in communication signal design (Lu FP et al., 2025; Xu ZC et al., 2025). As a class of orthogonal functions, PSWFs provide optimal energy concentration for a given time–bandwidth product. Recent advances in PSWF-based communication signal design are noteworthy. For instance, Xu ZC et al. (2025) proposed a generalized multimode PSWF-based multicarrier index modulation method that improves spectral efficiency via index modulation. However, their method is primarily intended for multicarrier transmission scenarios, where the waveform design objective fundamentally differs from that of the DSSS systems considered in the present study. In multicarrier systems, additional information is conveyed through subcarrier indexing, whereas the core goal of spread spectrum systems is to enhance chip waveform energy concentration and information mapping dimensionality.

PSWFs exhibit excellent properties such as completeness under finite time–bandwidth products and high-energy concentration (Slepian and Pollak, 1961; Osipov et al., 2013). As fundamental waveforms, they have been successfully used in ultrawideband communications, partial response modulation, and multicarrier modulation systems. Thus, they provide new avenues for enhancing the energy concentration of basic DSSS chip waveforms and expanding the dimensionality of information mapping.

Motivated by this, this study introduces PSWFs for fundamental chip waveform design and proposes a four-dimensional (4D) spread spectrum chip waveform design method based on PSWFs. First, starting from the relationship between information transmission efficiency and waveform dimension, the upper bound on the waveform dimension under time–bandwidth product constraints is derived. Second, PSWFs are used to construct a 4D orthogonal chip waveform set, and two implementation methods are proposed: a definition-based method and an equivalent low-pass filter (LPF)-based method. Furthermore, a corresponding spread spectrum modulation and demodulation system model and a low-complexity equivalent baseband implementation model are established. Finally, using simulations, the proposed method is compared with conventional chip waveforms in terms of power spectral characteristics, spectral efficiency, error performance, interference resistance, and anti-interception capability, confirming its performance advantages. The primary contributions of this study can be summarized as follows:

1. We derive the upper bound of four on the dimension of spread spectrum chip waveforms under time–bandwidth product constraints. By introducing PSWFs into the spread spectrum chip waveform design and proposing a PSWF-based method for constructing a 4D chip waveform set, the waveform dimension and spectral efficiency of spread spectrum systems are enhanced.

2. We construct a PSWF-based spread spectrum modulation and demodulation system model. By introducing equivalent low-pass processing, an equivalent low-pass PSWF spread spectrum system model is developed, where signal processing employs a “baseband+ in-phase/quadrature (I/Q) dual-channel” approach, effectively reducing implementation complexity.

3. We systematically analyze the proposed method in terms of power spectral characteristics, information transmission efficiency, error performance, interference resistance, and interception resistance. The results demonstrate that compared with spread spectrum modulation using rectangular, raised-cosine, or half-sine chip waveforms, the proposed method achieves higher information transmission efficiency and superior anti-interference and anti-interception capabilities, albeit with a moderate tradeoff in power efficiency. Consequently, it provides a chip waveform with an overall superior performance for spread spectrum modulation.

2 Design of the spread spectrum chip waveform set based on PSWFs

This section first analyzes the relationship between the spread spectrum chip waveform dimension and information transmission efficiency under time–bandwidth product constraints and derives the upper bound on the spread spectrum chip waveform dimension set. Based on this analysis, a 4D spread spectrum chip waveform set is constructed using PSWFs, following their definition and fundamental characteristics.

2.1 Analysis of the spread spectrum chip waveform dimension and information transmission efficiency

Assuming that a single-chip waveform has duration T and bandwidth W, the relationship between spread spectrum modulation information transmission efficiency η (bit/(s·Hz)) and chip waveform dimension N can be defined as follows:

$$\eta=\frac{Nm_{\mathrm{e}}}{WT}, \tag{1}$$

where m_e denotes the information capacity of a single chip. For conventional spread spectrum modulation employing rectangular pulse functions as chip waveforms, the chip waveform duration T (s) and bandwidth W (Hz) are constrained by the following relationship:

$$WT=2 \text{ Hz·s}. \tag{2}$$

Based on Eq. (1), the information transmission efficiency of the spread spectrum modulation can be improved by either increasing the chip waveform dimension N or adopting higher-order modulation to enhance the per-chip information capacity m_e. Given the linear relationship between chip waveform dimension and information transmission efficiency and the potential for additional efficiency gains through integration with higher-order modulation, the focus naturally shifts to increasing the chip waveform dimension to enhance spread spectrum modulation efficiency. In a traditional spread spectrum chip waveform design, the rectangular pulse function uses only one dimension, i.e., N=1, which fundamentally limits the information transmission efficiency. According to the Shannon–Nyquist sampling theorem, within duration T and bandwidth W, the maximum spatial dimension of a sampled signal is $2WT$. This implies that under the constraints of finite duration T and bandwidth W with the corresponding time–bandwidth product condition WT= 2 Hz·s, the maximum dimensionality of spread spectrum chip waveforms usable for information transmission is four.

Notably, according to the uncertainty principle, no orthogonal function exists that is fully constrained to duration T and bandwidth $2/T$ within the time–bandwidth product constraint of 2 Hz·s. As a class of non-sinusoidal functions, band-limited PSWFs with bandwidth W exhibit the highest-energy concentration within a finite duration T. This provides a new direction for designing high-energy concentration 4D spread spectrum code waveforms.

2.2 Construction of the 4D spread spectrum code waveform set based on PSWFs

Given the flexible controllability of PSWFs in terms of time width, bandwidth, and spectrum, this subsection proposes a method for constructing a PSWF-based chip waveform set using the PSWF defining formula. To reduce the complexity of constructing the chip waveform set, the equivalent low-pass principle is introduced, yielding a construction method based on equivalent low-pass filtering.

2.2.1 PSWF definition and fundamental characteristics

PSWFs are a unique class of non-sinusoidal wave functions that can be expressed in integral form for arbitrary values of time and frequency (Murugesan et al., 2023):

$$\int_{-T/2}^{T/2}\varphi_n(c,\tau)\frac{\sin\left(2\pi W(t-\tau)\right)}{\pi(t-\tau)}\mathrm{d}\tau=\lambda_n\varphi_n(c,t),\ n=0,1,2,\cdots. \tag{3}$$

Here, $t\in[-T/2, T/2]$ denotes the time, $c=TW$ (Hz·s) denotes the time–bandwidth product, $\varphi_n(c,t)$ denotes the n^{th}-order baseband PSWFs, and λ_n denotes the eigenvalues of $\varphi_n(c, t)$. By modifying the kernel function of the differential equation, passband PSWFs can be expressed integrally for arbitrary values of

$$\int_{-T/2}^{T/2}\varphi_n(c,\tau)\left[\frac{\sin\left(2\pi f_h(t-\tau)\right)}{\pi(t-\tau)}-\frac{\sin\left(2\pi f_l(t-\tau)\right)}{\pi(t-\tau)}\right]\mathrm{d}\tau=\lambda_n\varphi_n(c,t), \tag{4}$$
$$n=0,1,2,\cdots,$$

where f_h and f_l denote the upper and lower cutoff frequencies of the passband PSWFs, respectively. Furthermore, based on the principle of equivalent low-pass filtering, a passband PSWF $\varphi_{P,n}(c,t)$ with a center frequency $f_c=(f_h+f_l)/2$ and time–bandwidth product TW corresponds to a baseband PSWF $\varphi_{B,n}(c,t)$ with time–bandwidth product TW. The relationship between these two PSWFs can be expressed as follows:

$$\begin{aligned}&\varphi_{B,n}(c,t)\left\{\cos(2\pi f_c t),\sin(2\pi f_c t)\right\}\\&=\left\{\varphi_{P,2n}(c,t),\varphi_{P,2n+1}(c,t)\right\},\ n=0,1,2,\cdots.\end{aligned} \tag{5}$$

To illustrate the derivation of this equivalent low-pass structure more explicitly, we expand the complex envelope relationship in Eq. (5). Let the baseband PSWFs be denoted as $\varphi_0(t)$ and $\varphi_1(t)$, with a carrier frequency f_c. According to the bandpass-to-baseband conversion relationship in Eq. (5), the bandpass PSWF signal can be expressed as the real part of the baseband complex envelope as follows:

$$\varphi_{P,n}(c,t)=\mathrm{Re}\left\{\varphi_{B,n}(c,t)\,\mathrm{e}^{\mathrm{j}2\pi f_c t}\right\},\ n=0,1. \tag{6}$$

Expanding the complex exponential and separately extracting the orthogonal components of the real and imaginary parts yield four mutually orthogonal bandpass real signals derived from the two baseband PSWF functions:

$$\begin{cases}\varphi_{P,0}(c,t)=\varphi_{B,0}(c,t)\cos\left(2\pi f_c t\right),\\ \varphi_{P,1}(c,t)=\varphi_{B,0}(c,t)\sin\left(2\pi f_c t\right),\\ \varphi_{P,2}(c,t)=\varphi_{B,1}(c,t)\sin\left(2\pi f_c t\right),\\ \varphi_{P,3}(c,t)=\varphi_{B,1}(c,t)\cos\left(2\pi f_c t\right).\end{cases} \tag{7}$$

Thus, the 4D bandpass PSWF waveform set is not obtained by mapping via the multiplication of baseband PSWFs with orthogonal carriers, but rather by directly solving high-order bandpass numerical waveforms. Since the proposal of PSWFs, their fundamental characteristics have been extensively investigated. Many of these characteristics, such as complete orthogonality, high time–frequency energy concentration, and flexibility in time width, bandwidth, and spectrum, are highly valuable for signal processing applications, including waveform design, information loading, and detection.

2.2.2 Design of the 4D PSWF spread spectrum code waveform set

Based on Eqs. (3)–(5), under the constraint of time–bandwidth product WT=2 Hz·s, two approaches can be employed to design the 4D PSWF spread spectrum code waveform set: direct design based on definition and equivalent LPF design. The specifics are as follows:

1. Definition-based 4D PSWF spread spectrum code waveform set construction method

Leveraging the flexible and controllable spectral characteristics of PSWF signals, the 4D PSWF spread spectrum chip waveform set can be directly designed within the corresponding duration and frequency band of the measurement and control system, as illustrated in Fig. 1. The specific steps are as follows:

Step 1: set the system parameters, namely, signal duration T, signal bandwidth W, and spectral range (f_h,f_l);

Step 2: substitute the parameters from step 1 into Eq. (4) to obtain the numerical solutions of the 0^{th}–3^{rd}-order PSWF signals within the spectral range (f_h, f_l), signal duration T, and bandwidth W;

Step 3: combine the numerical solutions of the 0^{th}–3^{rd}-order PSWF signals into a PSWF chip waveform set:

$$\{\varphi_0(c,t),\varphi_1(c,t),\varphi_2(c,t),\varphi_3(c,t)\}. \quad (8)$$

For example, under constraints of a center frequency of 20 MHz, a bandwidth of 2 MHz, and a chip time width of 1 μs, four mutually orthogonal PSWF functions can be designed based on the relationship between the time–bandwidth product and the signal spatial dimension. The 0^{th}-, 1^{st}-, 2^{nd}-, and 3^{rd}-order PSWF functions are denoted as $\varphi_0(c, t)$, $\varphi_1(c, t)$, $\varphi_2(c, t)$, and $\varphi_3(c, t)$, respectively, as shown in Figs. 2 and 3.

2. Method for constructing the 4D PSWF chip waveform set based on equivalent LPFs

According to the equivalent LPF principle, for the 4D PSWF chip waveform set designed directly by definition, its corresponding two-dimensional (2D) baseband waveforms within the baseband can be obtained by up-conversion to generate the 4D PSWF spread spectrum chip set. Therefore, first, a 2D baseband PSWF chip waveform set with a center frequency of 0 Hz, bandwidth of $1/T$, and chip duration of T can be designed. Then, according to Eq. (5), by multiplying the sine carrier $\sin(2\pi f_c t)$ and cosine carrier $\cos(2\pi f_c t)$ with the 0^{th}-order and 1^{st}-order PSWF functions, respectively, the 4D PSWF chip waveform set can be obtained, as shown in Fig. 4.

Fig. 5 shows the design of the 4D PSWF signal set based on the equivalent LPF principle. The baseband PSWF signal has a bandwidth of 2 MHz, chip duration of 1 μs, and carrier center

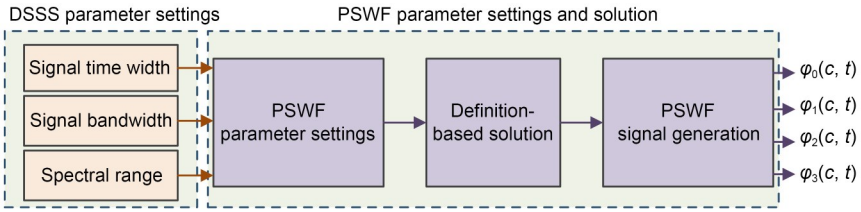


Fig. 1 Construction of the 4D PSWF code-sheet waveform set based on definitional formulas

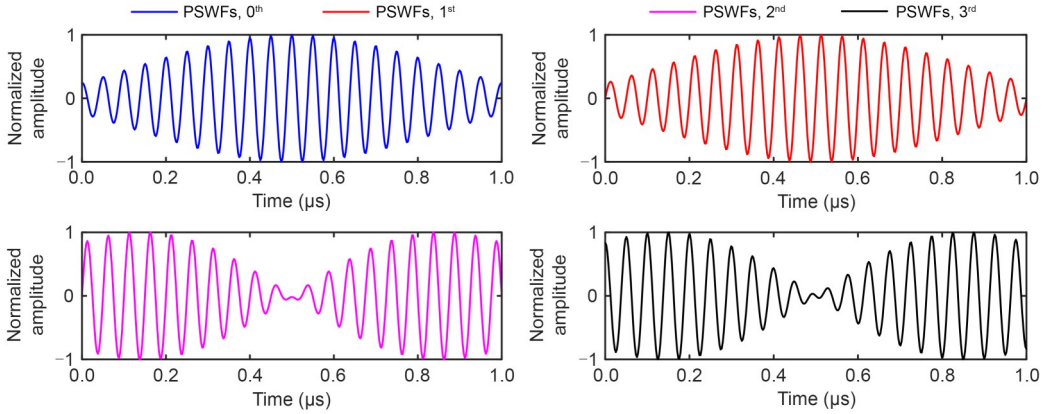


Fig. 2 Time-domain waveforms of PSWFs

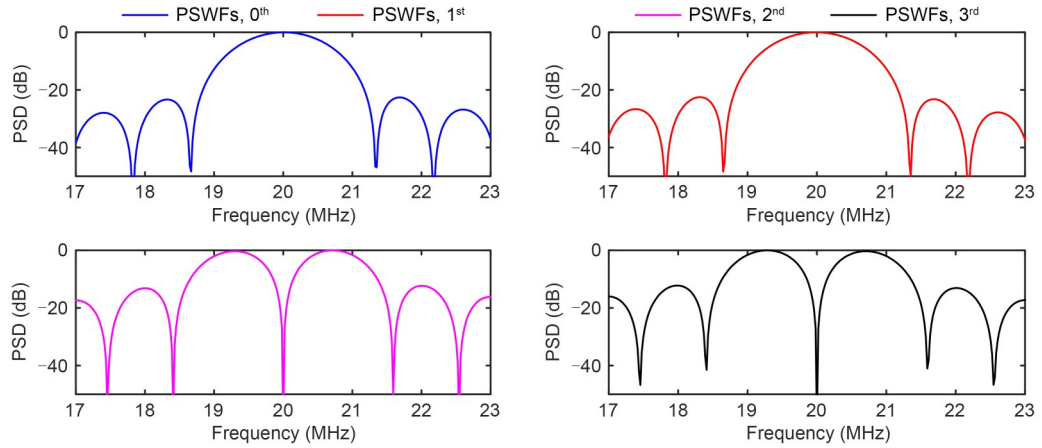


Fig. 3 Power spectrum of PSWFs. PSD: power spectral density

frequency of 10 MHz. The I/Q generation structures shown in Figs. 4 and 5 correspond to the four mutually orthogonal bandpass real signals derived from Eq. (7). Therefore, the equivalent low-pass structure is a natural mathematical equivalent of the waveform generation process rather than an additional approximation.

Numerical approximation methods are currently employed because closed-form analytic solutions do not exist for PSWF signals. However, these methods are computationally complex. The proposed design approach simplifies the process by requiring numerical solutions only for the first two orders of baseband PSWF signals, effectively expanding the PSWF signal set from two baseband waveforms to four passband dimensions. According to the equivalent LPF principle, the baseband numerical solutions remain unchanged for PSWF signals with identical bandwidth and duration but different center frequencies. Thus, by altering the up-conversion center frequency, a 4D PSWF spread spectrum chip waveform set with different center frequencies can be obtained. Consequently, compared with the definition-based design method, the equivalent low-pass design method achieves lower system implementation complexity.

3 Fundamental principles of PSWFs-based spread spectrum modulation

Based on the 4D PSWF chip waveform set, this section constructs a spread spectrum modulation system model using PSWF chip waveforms. A spread spectrum modulation model based on PSWF chip waveforms is established, followed by a corresponding demodulation model for the spread spectrum signal.

3.1 Spread spectrum modulation model based on PSWF chip waveforms

The spread spectrum modulation model based on PSWF chip waveforms comprises three modules: serial-to-parallel conversion, modulation symbol mapping and spread spectrum code generation, and PSWF waveform modulation (Fig. 6). The generation process of the spread spectrum modulation signal is as follows:

1. Serial-to-parallel conversion. The tracking, telemetry, and command (TT&C) data slated for transmission undergo serial-to-parallel conversion. Specifically, the data are transformed from serial to four parallel streams, each representing data index within streams, denoted as $d_0(j)$, $d_1(j)$, $d_2(j)$, $d_3(j)$, where the chip index j=0, 1, ⋯, N_c−1 with N_c denoting the length of the spreading code.

2. Bipolar phase–amplitude modulation (BPAM) mapping. After serial-to-parallel conversion, BPAM is applied to the binary data. This operation, also known as code conversion, transforms binary data of 0 s and 1 s into bipolar codes of +1 s and −1 s, denoted as $d_0'(j)$, $d_1'(j)$, $d_2'(j)$, $d_3'(j)$.

3. Spreading modulation. The same spreading code sequence is used to spread four bipolar data streams, generating four discrete baseband spread chip sequences. We define the spread symbol of the m^{th} (m=0, 1, 2, 3) channel at the $(j+1)^{\text{th}}$ chip position as follows:

$$a_m(j)=d_m'(j)\,c(j),\ m=0,1,2,3, \tag{9}$$

where $c(j)$ signifies the $(j+1)^{\text{th}}$ chip in the spread spectrum modulation code element.

4. PSWF waveform modulation. 0^{th}–3^{rd}-order PSWFs are used to modulate the four streams of digital baseband spread signals. Then, these modulated signals are combined to produce the radio frequency (RF) transmission signal, expressed as follows:

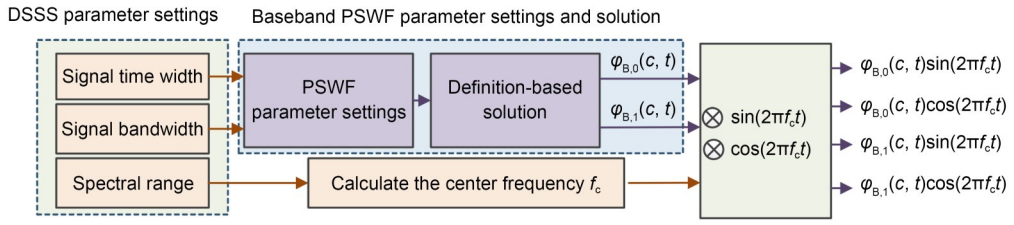


Fig. 4 Construction schematic of the 4D PSWF code-piece signal set based on equivalent LPFs. ⊗ denotes multiplication

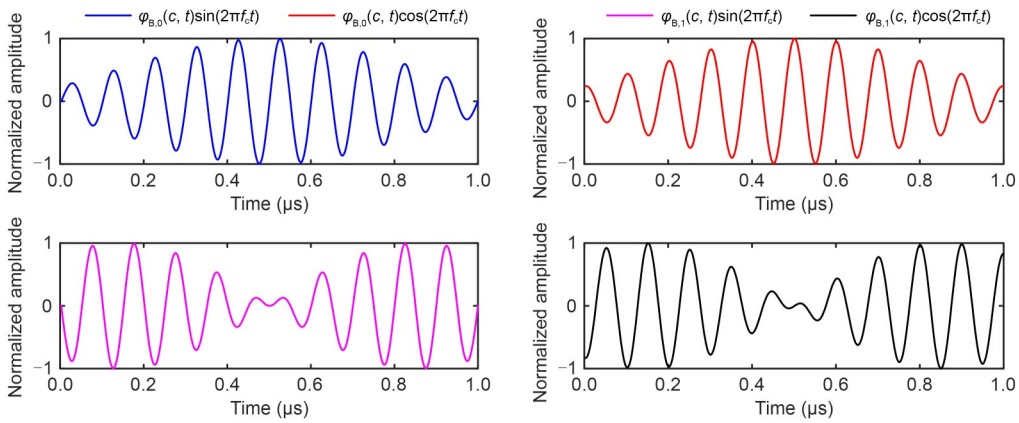


Fig. 5 Schematic of 4D PSWF time-domain waveforms based on equivalent LPFs

$$s(t)=\sum_{m=0}^{3}\sum_{j=0}^{N_c-1}a_m(j)\varphi_m(c,t-jT). \tag{10}$$

Here, $\varphi_m(c,t-jT)$ denotes the $(j+1)^{\text{th}}$ chip waveform of the m^{th}-order PSWF waveform after being shifted in time by jT. The relationship between the spreading modulation symbol length T_s and chip length is expressed as follows:

$$T_s=N_cT. \tag{11}$$

3.2 Spread spectrum signal demodulation model based on PSWF chip waveforms

The spread spectrum signal demodulation model based on PSWF chip waveforms primarily comprises three modules: PSWF-based signal detection, despreading and modulation symbol demapping, and parallel-to-serial conversion (Fig. 7).

First, the received signal is processed individually with the 0^{th}–3^{rd}-order PSWFs to obtain four chip data streams. Second, the chip data are integrated over the spreading code duration, and a decision is made, yielding four demodulated data streams. Finally, parallel-to-serial conversion is employed to reconstruct the modulated data for the TT&C system.

Notably, TT&C systems commonly function within microwave frequency bands. The elevated operating frequencies necessitate advanced digital processing and data access devices for the direct generation of microwave-band PSWF signals. Consequently, the system models shown in Figs. 6 and 7, which are designed to directly produce RF signals, encounter difficulties that hinder their feasibility in high-frequency applications. To address this challenge, we construct a low-complexity system implementation based on equivalent low-pass filtering.

3.3 Equivalent low-pass-based PSWF spread spectrum modulation implementation model

Building on the 4D PSWF chip waveform set derived from equivalent low-pass filtering, we establish an equivalent low-pass PSWF-based spread spectrum modulation model (Fig. 8). The key differences between the data presented in Figs. 6 and 8 are as follows:

1. PSWF waveform modulation. The 0^{th}- and 1^{st}-order baseband PSWFs, both with a time–bandwidth product of 1 Hz·s, are

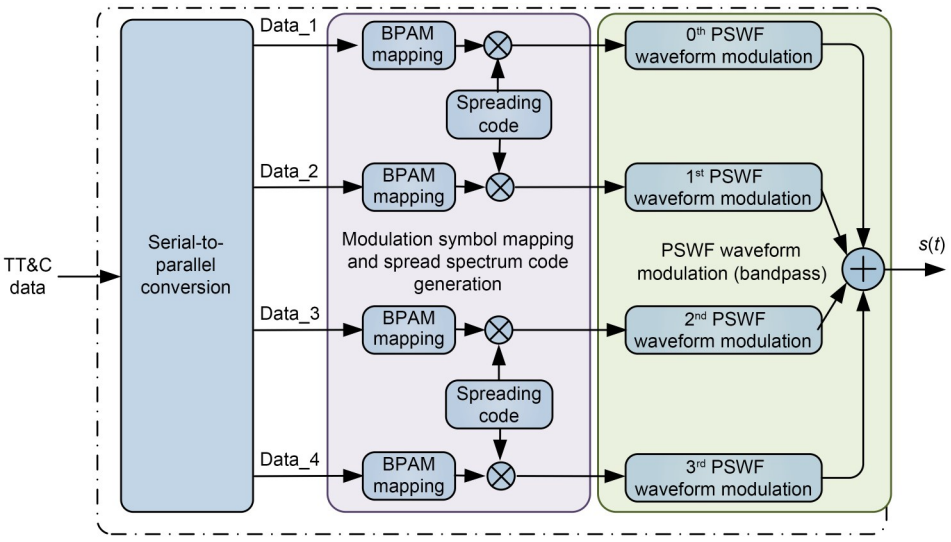


Fig. 6 Modulation model of the 4D unified spread spectrum TT&C system based on PSWF waveform modulation

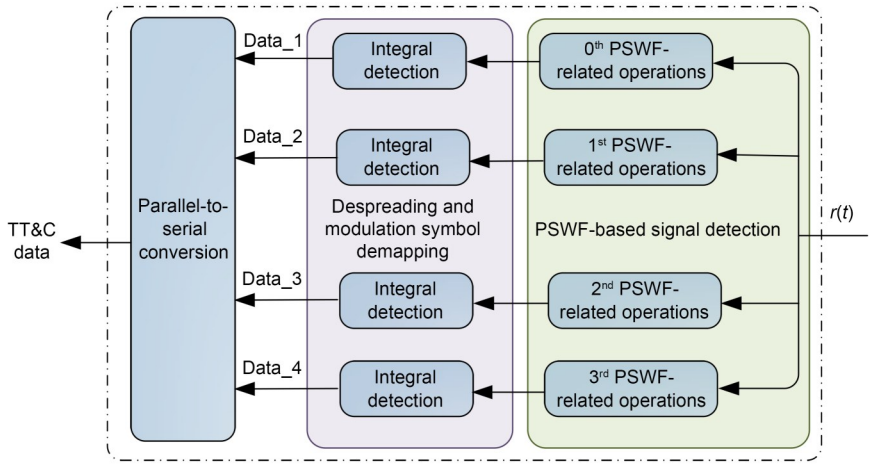


Fig. 7 Block diagram of the spread spectrum signal demodulation model based on PSWF code sequence waveform

used to modulate the first two and the last two digital baseband spread spectrum signals, respectively. Subsequently, the signals of the first two channels are superimposed to form the I-path signal, and those of the last two channels are superimposed to form the Q-path signal.

2. Carrier modulation. Sine and cosine carriers modulate the I- and Q-path signals, respectively. The modulated signals are then combined to produce the RF signal.

Subsequently, an equivalent low-pass PSWF-based spread spectrum demodulation model is constructed (Fig. 9). The key differences between the data presented in Figs. 7 and 9 are as follows: the down-conversion module transforms the received RF signal into baseband I and Q channel signals, which then undergo analog-to-digital converter (ADC). The demodulation and detection module performs matched-filter demodulation using the 0^{th}- and 1^{st}-order baseband PSWFs in the two channels, yielding four baseband data streams. Subsequently, parallel-to-serial conversion is used to recover the demodulated data.

Compared with direct RF generation methods based on the definition-based approach, the proposed equivalent low-pass implementation structure offers significant complexity advantages at the transmitter and receiver. At the transmitter, the proposed method only generates the 0^{th}- and 1^{st}-order PSWF waveforms at the baseband and employs orthogonal up-conversion for 4D expansion, thereby avoiding the stringent demands on digital-to-analog converter (DAC) sampling rates and high-speed field-programmable gate array (FPGA) resources imposed by directly solving for and generating high-order bandpass PSWFs at high frequencies. At the receiver, down-conversion shifts the signal processing band to the baseband, enabling core operations such as matched filtering, chip synchronization, and despreading to be performed in the low-speed digital domain and substantially reducing the requirements for ADC quantization bandwidth and subsequent baseband processing computations. Consequently, the proposed structure effectively alleviates implementation bottlenecks at microwave frequencies while balancing the high gain of 4D spreading with practical hardware feasibility.

Furthermore, the complexity reduction achieved by the equivalent low-pass structure differs between the transmitter and receiver.

1. Transmitter. The direct definition-based method requires generating the 0^{th}–3^{rd}-order bandpass PSWFs directly at RF or intermediate frequency, which imposes extremely stringent demands on the DAC sampling rate and the high-speed multiplication–accumulation resources of the FPGA. In contrast, the equivalent low-pass method

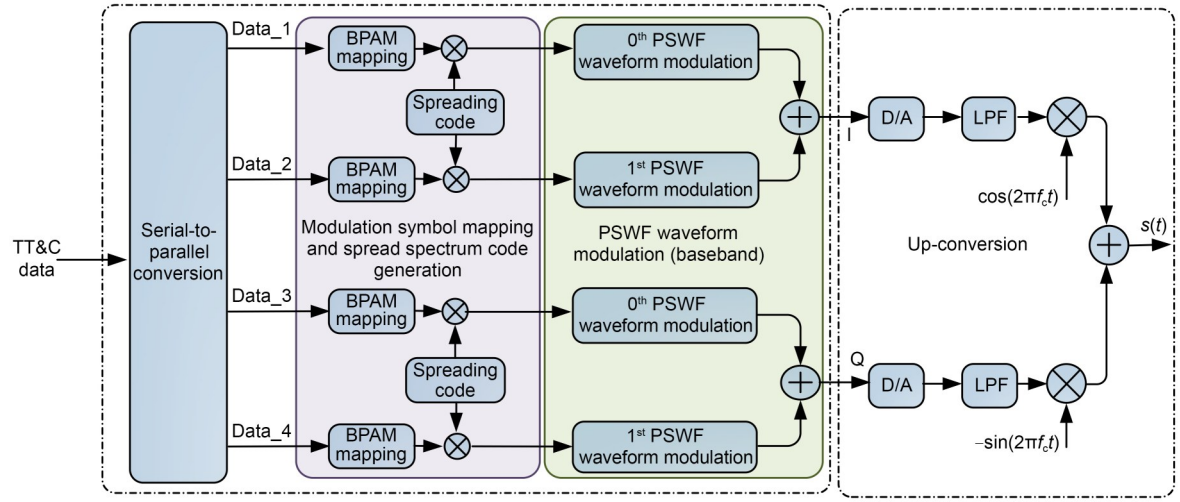


Fig. 8 Block diagram of the PSWF spread spectrum modulation based on equivalent LPFs. D/A: digital-to-analog. ⊕ denotes addition

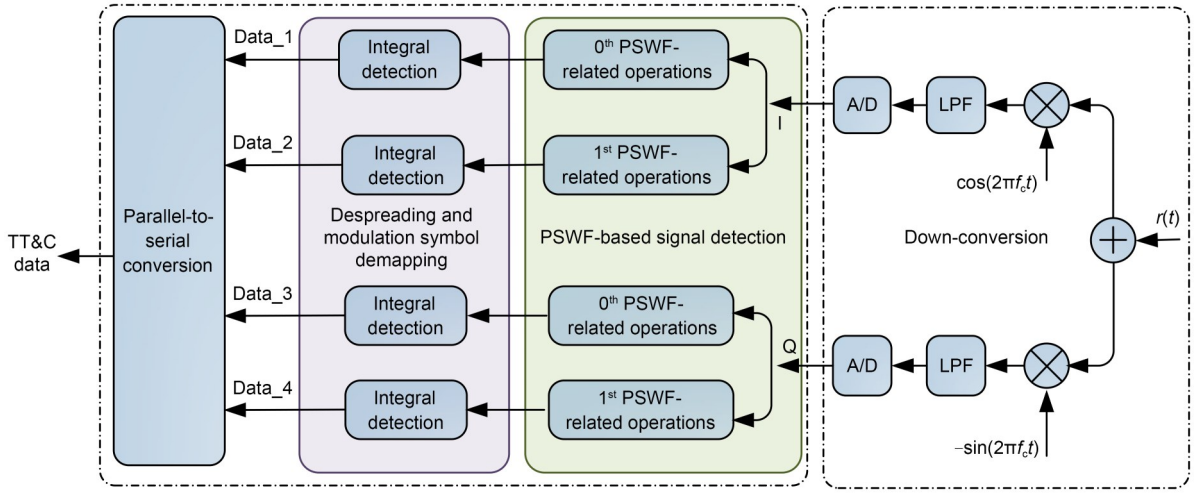


Fig. 9 Block diagram of the PSWF spread spectrum signal demodulation based on equivalent LPFs. A/D: analog-to-digital

generates only two waveforms at baseband (0^{th} and 1^{st} orders) and extends them to four dimensions via quadrature up-conversion (I/Q modulation). This approach significantly alleviates the burden on high-speed DAC resources and real-time numerical computation.

2. Receiver. If matched filtering is performed directly at bandpass, high-frequency analog components and ultra-high-speed ADCs would be required for bandpass sampling. The equivalent low-pass method first down-converts the signal to the baseband; subsequent matched filtering, synchronization, and aggregation are performed in the baseband digital domain. This approach not only relaxes the ADC sampling rate requirement but also allows the use of low-speed, high-precision baseband digital signal processors for parallel correlation operations.

4 System performance analysis

Because conventional spread spectrum chip waveforms are predominantly rectangular with raised-cosine and half-sine pulse functions, this section compares the proposed method with conventional spread spectrum chip waveforms across five aspects: power spectral characteristics, system information transmission efficiency, error rate performance, anti-interference performance, and anti-interception performance.

4.1 Signal power spectrum analysis

Fig. 10 presents the power spectra of different spread spectrum modulated signals. The main-lobe bandwidth of the 4D PSWF-based spread spectrum modulation signal (DS-PSWFs-4D) exceeds the designed signal bandwidth of 2.046 MHz, reaching approximately 3.2 MHz. Moreover, as the PSWF chip waveform dimension decreases (DS-PSWFs-1D/2D/3D), the main-lobe width narrows progressively and the first sidelobe diminishes. This indicates that the bandwidth of the receiver front-end filter affects the effective received signal power. The impact can be mitigated by reducing the PSWF chip dimension, albeit at the cost of spectral efficiency. Therefore, a key question arises: how does the front-end filter bandwidth affect the 4D PSWF-based spread spectrum modulation signal?

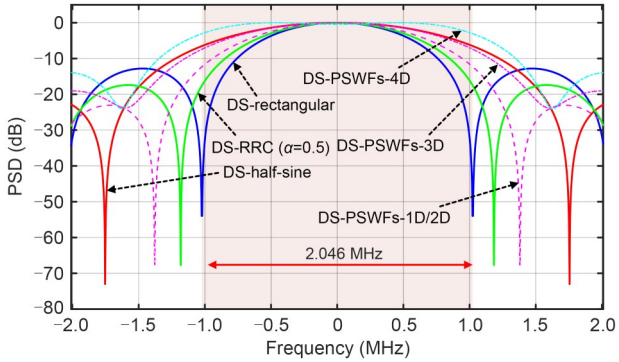


Fig. 10 Power spectrum diagrams of different spread spectrum modulation signals. PSD: power spectral density

Because the receiver front-end filter bandwidth affects the signal, resulting in energy loss and system performance degradation, the following analysis examines the impact of this filtering. The signal-to-noise ratio (SNR) loss due to the receiver filter bandwidth characteristics is denoted by

$$\zeta=\frac{\int_{-\infty}^{+\infty}S(f)\,\mathrm{d}f-\int_{-B_r/2}^{B_r/2}S(f)\,\mathrm{d}f}{\int_{-\infty}^{+\infty}S(f)\,\mathrm{d}f}, \tag{12}$$

where B_r denotes the receiver filter bandwidth, and $S(f)$ denotes the power spectral density of the target signal. A smaller value of ζ for the spread spectrum modulation signal results in a smaller SNR loss.

Fig. 11 shows the relationship between the SNR loss of spread spectrum modulation signals using different chip waveforms and filter bandwidths. The simulation results indicate that a narrower receiver front-end bandwidth results in a larger SNR loss, and this loss decreases progressively as the bandwidth increases. At a receiver filter bandwidth of 2 MHz, the proposed method exhibits the highest SNR loss compared with spread spectrum modulation using rectangular, half-sine, and root-raised-cosine (RRC, roll-off factor α=0.5) chip waveforms. When the receiver filter bandwidth exceeds 5 MHz, the proposed method yields a lower SNR loss than spread spectrum modulation using the same three-chip waveforms.

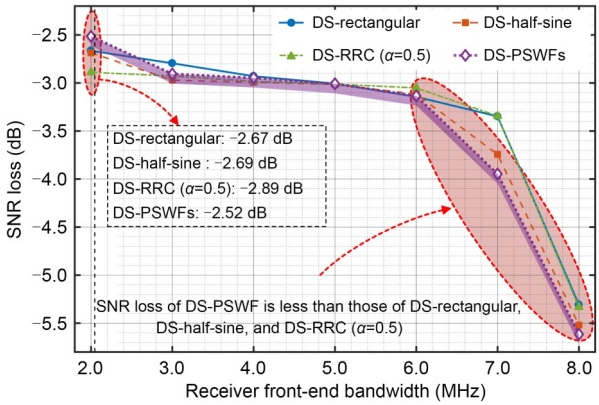


Fig. 11 SNR loss due to the receiver filter bandwidth

The above analysis demonstrates that the effect of the receiver front-end filter bandwidth on the 4D PSWF-based spread spectrum modulation signal can be mitigated by reducing the dimension of the PSWF chip waveform or by increasing the reception bandwidth.

4.2 Analysis of system information transmission efficiency

Under fixed transmission bandwidth W and bit error rate (BER) P constraints, for spread spectrum modulation using traditional chip waveforms, such as rectangular window, raised-cosine, or half-sine pulses with I/Q dual-channels, the spectral efficiency C_{DS}/W is proportional to the inverse of the spread factor K, satisfying the following relationship:

$$C_{DS}/W \propto 1/K. \tag{13}$$

Here, C_{DS} denotes the spread spectrum modulation information transmission efficiency under W and P constraints, and K represents the spectrum expansion factor, where a larger K value results in lower spectral efficiency.

For spread spectrum modulation using 4D PSWF spread spectrum code waveforms, because they have a code waveform dimension of four, which is twice that of traditional code waveforms, the system transmission efficiency doubles when K is large. Under identical constraints, the transmission efficiency is given by

$$C_{\text{DS-PSWFs}}=2C_{\text{DS}}. \tag{14}$$

Therefore, the spectral efficiency $C_{\text{DS-PSWFs}}/W$ of 4D PSWF-based spread spectrum modulation is proportional to twice the inverse of the spread factor K, satisfying the following relationship:

$$C_{\text{DS-PSWFs}}/W \propto 2/K. \tag{15}$$

Fig. 12 illustrates the relationship between the spectral efficiency and the inverse of the spreading factor for systems using different spreading code waveforms. The transmission efficiency of 4D PSWF-based spreading modulation is twice that of traditional spreading modulation.

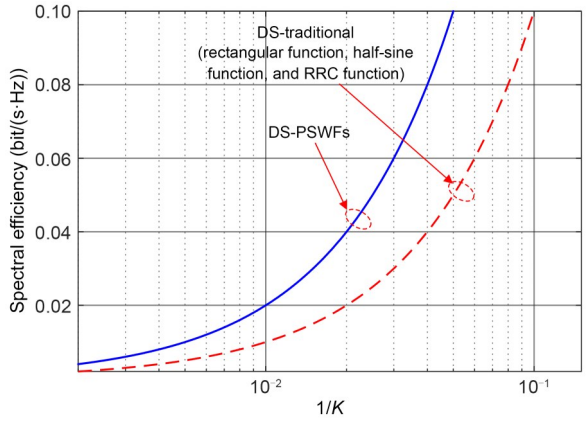


Fig. 12 Relationship between the spread spectrum modulation spectral efficiency and the inverse of spread factor K

4.3 System BER performance analysis

Because the 4D chip waveforms used in PSWF-based quad-spread modulation are mutually orthogonal, the BER performance of different quadruple spread modulation signals remains identical under additive white Gaussian noise (AWGN) channels. For analytical convenience and non-generalizability, the BER performance of the system is analyzed using channel k (k=1, 2, 3, 4) as an example.

Under Gaussian white noise channels, the received signal can be expressed as follows:

$$r(t)=s(t)+n(t), \tag{16}$$

where $n(t)$ denotes the AWGN with a mean of 0 and a bilateral power spectral density of $N_0/2$. Coherent detection yields the detection quantity for receiver channel k as follows:

$$D_{d_k}=d_k+n_k, \tag{17}$$

where n_k denotes the noise-induced interference. Given the properties of Gaussian white noise, D_{d_k} follows a Gaussian distribution with mean d_k and variance $N_0/2$. Therefore, the detection error rate for channel k is given by

$$P_{\text{e},k}=\frac{1}{2}\operatorname{erfc}\left(\sqrt{\frac{E_\text{b}}{N_0}}\right), \tag{18}$$

where erfc(·) denotes the complementary error function, and E_b denotes the energy per bit.

The corresponding overall BER for the 4D PSWF-based spread spectrum modulation system is given by

$$P_\text{e}=\frac{1}{4}\sum_{k=1}^{4}P_{\text{e},k}=\frac{1}{2}\operatorname{erfc}\left(\sqrt{\frac{E_\text{b}}{N_0}}\right). \tag{19}$$

Furthermore, for spread spectrum modulation using conventional chip waveforms, such as rectangular windows, raised-cosine functions, or half-sine pulses, the system BER also follows Eq. (19). This indicates that the proposed method is comparable to conventional chip-waveform-based spread spectrum modulation in terms of BER performance; therefore, further discussion is omitted in this study.

Monte–Carlo simulations are performed to evaluate the error performance of the system. Fig. 13 shows the theoretical and simulated BER curves. The results demonstrate close agreement between the simulated and theoretical BERs, confirming the correctness of the theoretical BER analysis and the feasibility and superiority of the proposed method.

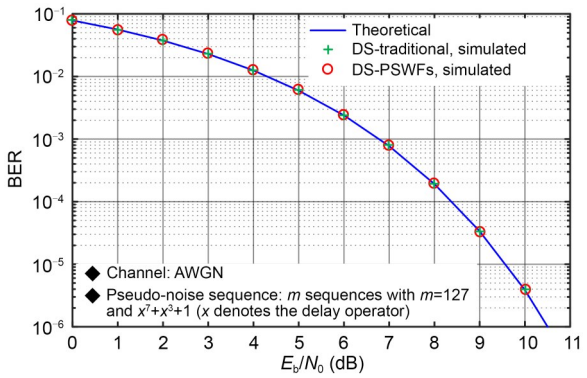


Fig. 13 Theoretical and simulated BER curves

4.4 System anti-interference performance

Fig. 14 shows the BER curves of the proposed method under equal-power interference from narrowband binary phase shift keying (BPSK)-modulated signals, wideband BPSK-modulated signals, and other DSSS-modulated signals. All three interference types degrade error performance, with wideband interference causing the most significant degradation, followed by other DSSS signals and narrowband interference. This result demonstrates that the proposed method effectively resists narrowband, wideband, and cochannel spread spectrum interferences, providing important guidance for practical applications.

4.5 System anti-interception performance

The anti-interception performance analysis discussed in this study is predicated on the following threat model assumptions: although the noncooperative intercepting receiver possesses knowledge of

fundamental RF parameters, including the carrier frequency and bandwidth of the signal (which can be obtained using conventional methods such as spectrum scanning), it remains ignorant of the following critical information: (1) the precise order and waveform parameters (such as the exact values of the time–bandwidth product) of the PSWF basis functions; (2) the specific composition of the spread spectrum code sequence; (3) the particular waveform dimensions selected for information mapping within the 4D PSWF waveform set employed by the transmitter. This assumption is consistent with the security design principles inherent in practical spread spectrum communication systems, where system security predominantly relies on the confidentiality of keys (spread spectrum codes) and waveform parameters rather than the obfuscation of RF parameters. Notably, even if a noncooperative entity acquires prior knowledge of the PSWF basis functions, the proposed method retains its anti-interception superiority. The underlying rationale is the enhanced redundancy in signal space dimensions provided by the 4D PSWF waveform set.

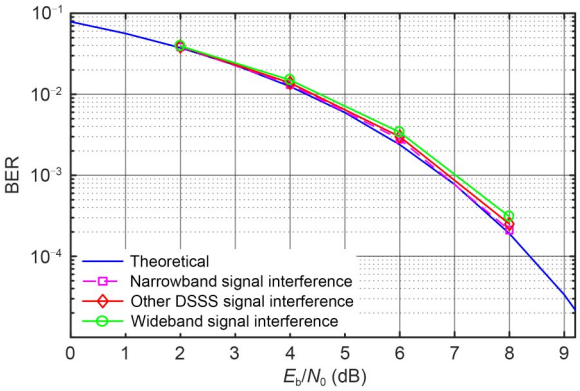


Fig. 14 Error rate simulation curves for system anti-interference capability

Notably, the preceding analysis is based on the assumption that the eavesdropper has no prior knowledge of the PSWF basis functions. Note that the proposed method also benefits from the inherent parameter flexibility of PSWFs (e.g., tunable time–bandwidth product and adjustable orders), which provides an extra layer of security when the eavesdropper does not possess exact knowledge of these parameters. However, to evaluate the anti-eavesdropping performance under more stringent conditions, we consider the worst-case scenario where the eavesdropper knows the PSWF basis functions, key system parameters (including the precise parameter values), and even the waveform dimension assignment. Even in this worst-case scenario, the proposed waveform still maintains its anti-eavesdropping advantage, primarily for the following two reasons:

First, the randomness of the spreading code provides the primary security guarantee. In DSSS systems, the core source of anti-eavesdropping capability lies in the randomness and long periodicity of the spreading code sequence. Even if an eavesdropper knows the PSWF basis functions, the spreading code sequence still needs to be obtained through blind estimation or exhaustive search. Under the same data rate and bandwidth conditions, the proposed method increases the spreading code sequence length from 1023 bits in conventional schemes to 2046 bits (Table 1), exponentially increasing the complexity of an exhaustive search.

Table 1 Comparison of design parameters

Parameter type	Traditional spread spectrum	4D PSWF-based spread spectrum modulation
Chip waveform	Rectangular window, rised-cosine function, half-sine pulse, etc.	4D PSWF-based code waveform
Chip waveform dimension	1 (baseband) 2 (bandpass)	2 (baseband) 4 (bandpass)
Chip length (s)	1/1.023e-6	1/1.023e-6
Bandwidth (MHz)	2.046	2.046
Information transmission efficiency (bit/s)	2000	2000
Chip symbol duration (s)	0.001	0.002
Chip bit count (bit)	1023	2046

Second, 4D waveform mapping increases the difficulty of signal sorting and identification. Conventional spread spectrum systems use only one-dimensional (or 2D I/Q) chip waveforms for information mapping, whereas this study employs a set of 4D orthogonal PSWF waveforms for mapping. After intercepting a signal, an eavesdropper must perform waveform detection and code sequence estimation simultaneously across four orthogonal dimensions, resulting in significantly higher complexity for signal sorting and parameter estimation than in conventional 2D systems.

Compared with conventional spread spectrum modulation using rectangular, raised-cosine, or half-sine pulse chip waveforms, the proposed method employs a 4D PSWF-based chip waveform, providing greater signal dimensionality and higher spectral efficiency. The following analysis demonstrates how these technical advantages are translated into enhanced anti-interception capability. To more intuitively illustrate system performance, we compare the anti-interception capabilities of conventional spread spectrum modulation and the proposed method under identical information transmission efficiency, transmission bandwidth, and BER requirements.

Assuming a telemetry system design requirement of a transmission bandwidth of 2.046 MHz and an information transmission efficiency of 2000 bit/s, the design parameters for the two approaches are listed in Table 1. The resulting anti-interception benefits manifest in two ways. First, the difficulty for a noncooperative party to intercept the telemetry signal is significantly increased primarily because the spreading code length is extended from 1023 to 2046 bits. Second, the system spreading gain increases from 30.1 to 33.1 dB, improving the anti-interference capability by 3 dB. Under identical non-Gaussian interference conditions, the transmission power can be reduced by 3 dB, thereby lowering the power spectrum of the signal by 3 dB and decreasing the probability of interception.

Compared with conventional schemes that rely on a single-chip waveform, the proposed 4D PSWF waveform set provides the following extended capabilities for multiuser access:

1. User differentiation in the waveform domain. In conventional CDMA systems, users are distinguished solely by spreading codes. The proposed method introduces the waveform dimension as an additional means of user differentiation beyond the spreading code. By assigning different combinations of PSWF waveform dimensions to users, the system can support more simultaneous users

while maintaining the same spreading code length or employ shorter spreading codes to increase data rates for the same number of users.

2. Multidimensional resource scheduling. The 4D PSWF waveform set, along with the spreading code sequences, forms a 2D resource pool (waveform dimension×code sequence). The system can dynamically allocate waveform dimensions and code resources according to users' quality-of-service requirements, enabling more flexible multiuser resource management.

3. Performance advantages under partial loading. When the system is underloaded (i.e., the number of active users is below the maximum supported number), different PSWF waveform dimensions can be preferentially assigned to users, enabling their signals to remain orthogonal or quasi-orthogonal in the waveform domain. This effectively reduces multiple access interference and improves BER performance.

5 Conclusions

To address the issues of low chip waveform dimensionality and insufficient spectral efficiency in conventional DSSS systems, this study proposes a 4D spread spectrum chip waveform design method based on PSWFs and constructs a corresponding spread spectrum modulation system implementation model. First, under the given time–bandwidth product constraints, spectral efficiency is enhanced by increasing the chip waveform dimension. A 4D orthogonal chip waveform set is constructed using PSWFs. Second, two approaches for chip waveform design and spread spectrum modulation system implementation, namely, definition- and equivalent LPF-based approaches, are proposed. These two approaches effectively reduce system implementation complexity. The simulation results demonstrate that the proposed waveform achieves approximately double the spectral efficiency of conventional waveforms while maintaining comparable error performance. It also exhibits robust anti-interference and anti-interception capabilities under narrowband, broadband, and cochannel spread spectrum signal interferences. However, this study has limitations, including the lack of waveform optimization for multipath channels and the high computational complexity of PSWF numerical solutions. Future work will focus on higher-dimensional PSWF waveform design, adaptation to frequency-selective channels, comprehensive performance evaluation in multiuser scenarios, and real-time verification using software-defined radio to advance the application of this technology in B5G/6G and integrated space–ground networks.

Acknowledgments

This work was supported by the Shandong Provincial Natural Science Foundation (No. ZR2023MD045) and the China National Postdoctoral Program for Innovative Talents (No. BX20200039).

Author contributions

Zhichao XU, Faping LU, and Zhilin ZHANG designed the research, processed the data, and drafted the paper. Zhongyang MAO, Dongkai YANG, and Jiafang KANG helped organize the paper. Zhongyang MAO, Fucheng YANG, and Feng WANG revised and finalized the paper.

Conflict of interest

All the authors declare that they have no conflict of interest.

Data availability

The data that support the findings of this study are available from the corresponding author upon reasonable request.

Declaration on the use of generative AI tools

During the preparation of this work, the authors used DeepSeek to improve language. After using this tool, the authors reviewed and edited the content as needed and take full responsibility for the content of the published article.

References

Cai XM, Huang CW, Chen PP, et al., 2025. Design of non-coherent RIS-empowered DCSK with two-level nested index modulation. *IEEE Trans Wirel Commun*, 24(4): 3044-3058. https://doi.org/10.1109/TWC.2025.3527499

Dai XM, Huang ZY, Luo YQ, et al., 2025. A low-complexity algorithm for designing waveforms with low weighted integrated sidelobe levels. *Wirel Pers Commun*, 140(1):453-466. https://doi.org/10.1007/s11277-024-11730-y

De Sanctis M, Cianca E, Rossi T, et al., 2015. Waveform design solutions for EHF broadband satellite communications. *IEEE Commun Mag*, 53(3):18-23. https://doi.org/10.1109/MCOM.2015.7060477

Dogukan AT, Basar E, 2026. Reconfigurable intelligent surface code index modulation with quadrature receive spatial modulation. *IEEE Trans Green Commun Netw*, 10: 522-532. https://doi.org/10.1109/TGCN.2025.3587881

Du J, Chen C, Zeng ZH, et al., 2025. Flexible waveform design for RO-ISAC based on OFDM-embedded maximum length sequence. *IEEE Wirel Commun Lett*, 14(10): 3334-3338. https://doi.org/10.1109/LWC.2025.3593253

Duan XD, Huang ZL, Liang SY, et al., 2025. AI-agent communication network for 6G: vision, architecture, and key technologies. *Front Inform Technol Electron Eng*, 26(11):2065-2080. https://doi.org/10.1631/FITEE.2500582

Han K, Meng KT, Masouros C, et al., 2026. MIMO-OFDM signaling design for non-coherent distributed ISAC systems. *IEEE Trans Wirel Commun*, 25:7792-7808. https://doi.org/10.1109/TWC.2025.3633615

He CL, Xiao LX, Li S, et al., 2025. Index modulation aided OTFS for SCMA system. *China Commun*, 22(8):19-28. https://doi.org/10.23919/JCC.ja.2023-0293

Huang GJ, Zhang SZ, Jin SG, et al., 2025. A novel multi-beam directional modulation OFDM waveform design for integrated sensing and communication. *IEEE Trans Veh Technol*, 74(11):18220-18225. https://doi.org/10.1109/TVT.2025.3576252

Hui Y, Tang KH, Liu KM, et al., 2026. Power and signal dual modulation in DC/DC converters using FSK-based DSSS for high anti-interference performance. *IEEE Trans Power Electron*, 41(3):3712-3725. https://doi.org/10.1109/TPEL.2025.3603575

Jin XP, Zhang P, Wan C, et al., 2023. RIS assisted dual-function radar and secure communications based on frequency-shifted chirp spread spectrum index modulation. *China Commun*, 20(10):85-99. https://doi.org/10.23919/JCC.fa.2023-0143.202310

Jin Y, Ji HB, 2011. A novel cyclic-moment based method for DS-SS QPSK signal blind parameter estimation. *Chin J Electron*, 20(4):686-690.

Jin Y, Deng ZL, Zhang H, et al., 2026. A review of UAV positioning in LAIN: toward a 5G-core "space–air–ground" integrated and cooperative architecture. *ENGINEERING Inform Technol Electron Eng*, 27(1):1-16. https://doi.org/10.1631/ENG.ITEE.2025.0127

Liu JC, Zhang JT, Li T, et al., 2025. Unintended interference suppression based on decision feedback adaptive cancellation for DSSS satellite communication. *Chin J Electron*, 34(2):673-682. https://doi.org/10.23919/cje.2023.00.398

Liu MZ, Liu J, Peng Z, et al., 2025. Efficient MMSE equalization for direct-sequence spread-spectrum underwater communications. *IEEE Internet Things J*, 12(11): 16325-16335. https://doi.org/10.1109/JIOT.2025.3532596

Lu FP, Zhang ZL, An Q, et al., 2025. A simplified fast Fourier transform algorithm. Proc 8th World Conf on Computing and Communication Technologies, p.176-179. https://doi.org/10.1109/WCCCT65447.2025.11028013

Lu ZW, Jiao YW, Chen YD, 2024. High stability code tracking for band-limited DSSS systems. *IEICE Trans Commun*, E107-B(11):706-718. https://doi.org/10.23919/transcom.2023EBP3201

Murugesan PPK, Sivabalin VPG, Nanjan SM, et al., 2023. Orthogonal modes using prolate spheroidal wave function in holographic communication systems. Proc Int Conf on Signal Processing, Computation, Electronics, Power and Telecommunication, p.1-6. https://doi.org/10.1109/IConSCEPT57958.2023.10170733

Ni ZT, Zhang JA, Liu RP, et al., 2026. Ambiguity function-based filter designs for OFDM ISAC systems. *IEEE Wirel Commun Lett*, 15:181-185. https://doi.org/10.1109/LWC.2025.3623243

Oh S, Moon H, 2024. Novel algorithm for joint channel estimation and spreading sequence detection in DSSS systems. *IEEE Access*, 12:128694-128701. https://doi.org/10.1109/ACCESS.2024.3449284

Osipov A, Rokhlin V, Xiao H, 2013. Prolate Spheroidal Wave Functions of Order Zero: Mathematical Tools for Bandlimited Approximation. Springer, New York, USA. https://doi.org/10.1007/978-1-4614-8259-8

Qian M, Ji F, Ge Y, et al., 2025. Generalized code index modulation aided AFDM for spread spectrum systems. *IEEE Wirel Commun Lett*, 14(10):3229-3233. https://doi.org/10.1109/LWC.2025.3589690

Sarwar MS, Ramatryana INA, Budiman G, et al., 2025. An uplink frequency-time index modulation multiple access for 6G networks. *IEEE Trans Veh Technol*, 74(5): 7866-7880. https://doi.org/10.1109/TVT.2025.3531012

Shao YZ, Zhang TQ, Yue PY, et al., 2026. Direct joint detection and localization of weak DSSS signals via cooperative LEO satellites. *IEEE Trans Commun*, 74:6571-6583. https://doi.org/10.1109/TCOMM.2026.3678430

Slepian D, Pollak HO, 1961. Prolate spheroidal wave functions, Fourier analysis and uncertainty–I. *Bell Syst Techn J*, 40(1):43-63. https://doi.org/10.1002/j.1538-7305.1961.tb03976.x

Su ZP, Zhang GF, Zhou XX, et al., 2021. Segment-adaptive spread spectrum audio watermarking using NSGA-II. *Chin J Electron*, 30(4):727-735. https://doi.org/10.1049/cje.2021.05.015

Todorović BM, Stojanović NM, Velikić GS, et al., 2024. Is direct sequence spread spectrum modulation promising for AI-based design of 6G networks? *IEEE Consum Electron Mag*, 13(5):7-10. https://doi.org/10.1109/MCE.2024.3349458

Vangelista L, Jechoux B, Canonici JX, et al., 2024. Golden modulation: a new and effective waveform for massive IoT. *IEEE Trans Commun*, 72(4):1938-1948. https://doi.org/10.1109/TCOMM.2023.3342821

Waheed A, Mohammady S, 2024. Spread spectrum OFDM-IM with efficient precoded matrix and low complexity detector. *IEEE Access*, 12:192293-192300. https://doi.org/10.1109/ACCESS.2024.3519446

Wang S, Song Z, Hua ZZ, et al., 2026. GaussMask-DSSS: enhancing covert spread spectrum communication with Gaussian cloaking and deep learning-aided synchronization. *IEEE J Sel Areas Commun*, 44:1495-1511. https://doi.org/10.1109/JSAC.2025.3637799

Xu YZ, Peng YY, Al-Hazemi F, et al., 2026. Dual-functional radar and communication system based on hybrid index modulation. *IEEE Wirel Commun Lett*, 15:1886-1890. https://doi.org/10.1109/LWC.2026.3662791

Xu ZC, Lu FP, Zhang LF, et al., 2025. Generalized multiple-mode prolate spheroidal wave functions multi-carrier waveform with index modulation. *J Syst Eng Electron*, 36(2):311-322. https://doi.org/10.23919/JSEE.2024.000044

Xue R, Xie MM, 2023. Partial response continuous phase modulation with a prolate spheroidal wave function for compass system in the S-band. *EURASIP J Adv Signal Process*, 2023(1):88. https://doi.org/10.1186/s13634-023-01052-9

Yan WH, An JP, Feng YB, et al., 2026. Coherent acquisition of MC-DSSS signal for LEO satellite communication. *IEEE Trans Commun*, 74:6395-6408. https://doi.org/10.1109/TCOMM.2026.3669498

Yang YX, Gao P, 2023. Design method of multi-layer multi-parameter multi-term weighted-type fractional Fourier transform composite modulation communication signal. *J Electron Inform Technol*, 45(4):1192-1200 (in Chinese). https://doi.org/10.11999/JEIT220266

Yang ZJ, Su W, Zhang HK, 2026. Overview of heterogeneous AMN architectures integrating satellite and terrestrial networks: a communication–sensing–computing perspective. *Chin J Aeronaut*, 39(5):103918. https://doi.org/10.1016/j.cja.2025.103918